INTERNATIONAL JOURNAL OF
RADIATION ONCOLOGY • BIOLOGY • PHYSICS
www.redjournal.org

CLINICAL INVESTIGATION

Potential Role of Lymphocyte CD44 in Determining Treatment Selection Between Stereotactic Body Radiation Therapy and Surgery for Early-Stage Non-Small Cell Lung Cancer

Weiwei Yan, MD,[*,†] Ziyuan Ren, MMed,[*,†] Xi Chen, MMed,[*,†] Ran Zhang, Ph.D.,[†] Juncai Lv, MMed,[†] Vivek Verma, MD,[‡] Meng Wu, Ph.D.,[†] Dawei Chen, MD,[*,†] and Jinming Yu, MD[*,†]

[*]*Cheeloo College of Medicine, Shandong University Cancer Center, Jinan, Shandong, China;* [†]*Department of Radiation Oncology and Shandong Provincial Key Laboratory of Radiation Oncology, Shandong Cancer Hospital and Institute, Shandong First Medical University and Shandong Academy of Medical Sciences, Jinan, Shandong, China; and* [‡]*Department of Radiation Oncology, University of Texas MD Anderson Cancer Center, Houston, Texas*

Received Jul 20, 2023; Accepted for publication Feb 12, 2024

Purpose: Stereotactic body radiation therapy (SBRT) versus surgery for operable early-stage non-small cell lung cancer (ES-NSCLC) remains highly debated. Herein, we used spatial proteomics to identify whether any molecular biomarker(s) associate with the efficacy of either modality, in efforts to optimize treatment selection between surgery and SBRT for this population.

Methods and Materials: We evaluated biopsy tissue samples from 44 patients with ES-NSCLC treated with first-line SBRT (cohort 1) by GeoMx Digital Spatial Profiling (DSP) with a panel of 70 proteins in 5 spatial molecular compartments: tumor (panCK+), leukocyte (CD45+), lymphocyte (CD3+), macrophage (CD68+), and stroma (α-SMA+). To validate the findings in cohort 1, biopsy samples from 52 patients with ES-NSCLC who received SBRT (cohort 2) and 62 patients with ES-NSCLC who underwent surgery (cohort 3) were collected and analyzed by multiplex immunofluorescence (mIF).

Results: In cohort 1, higher CD44 expression in the lymphocyte compartment was associated with poorer recurrence-free survival (RFS) (DSP: $P < .001$; mIF: $P < .001$) and higher recurrence rate (DSP: $P = .001$; mIF: $P = .004$). mIF data from cohort 2 validated these findings ($P < .05$ for all). From cohort 3, higher lymphocyte CD44 predicted higher RFS after surgery ($P = .003$). Intermodality comparisons demonstrated that SBRT was associated with significantly higher RFS over surgery in CD44-low patients ($P < .001$), but surgery was superior to SBRT in CD44-high cases ($P = .016$).

Conclusions: Lymphocyte CD44 may not only be a predictor of SBRT efficacy in this population but also an important biomarker (pending validation by large prospective data) that could better sharpen selection for SBRT versus surgery in ES-NSCLC.

Corresponding authors: Jinming Yu; and Dawei Chen; E-mail: dave0505@yeah.net, sdyujinming@163.com

Disclosures: This work was funded by the National Natural Science Foundation of China (82172676), the Natural Science Foundation of Shandong (ZR2021YQ52, ZR2020LZL016), and the Young Elite Scientist Sponsorship Program by Cast (no. YESS20210137).

Data Sharing Statement: Research data are stored in an institutional repository and will be shared upon request to the corresponding author.

Supplementary material associated with this article can be found in the online version at doi:10.1016/j.ijrobp.2024.02.048.

Acknowledgments—We thank all patients for participating in the study. We also thank Fynn Biotechnologies (Shandong) Ltd for their technical support with the DSP experiments and ShanDong PhenoScience Biotechnology Ltd for assisting in the automated cell quantification.

0360-3016/$ - see front matter
https://doi.org/10.1016/j.ijrobp.2024.02.048

Introduction

Owing to the institution of low-dose computed tomography (CT) screening, there has been an increase in the detection of early-stage non-small cell lung cancer (ES-NSCLC) cases.[1,2] Surgical lobectomy with mediastinal lymph node dissection remains the standard of care for medically operable patients, and stereotactic body radiation therapy (SBRT) has emerged as a preferred alternative for medically inoperable patients or those who refuse surgery.[3]

Even for operable patients with ES-NSCLC, multiple studies have shown SBRT may not be inferior to surgery. Two single-arm prospective studies in medically operable patients, RTOG 0618 and JCOG 04013, suggest favorable overall survival (OS) associated with SBRT compared with historical surgical outcomes.[4,5] A pooled analysis of 2 independent phase 3 trials, STARS and ROSEL (both prematurely closed due to poor accrual), comparing SBRT with surgery in patients with operable stage I NSCLC, showed superior OS with SBRT versus lobectomy (95% vs 79% at 3 years, $P = .037$).[6] The long-term results of the revised STARS trial showed that SBRT was noninferior to surgery in terms of OS and progression-free survival for patients with operable stage IA NSCLC.[7]

Given these recent findings, it is plausible that some operable SBRT patients could be better candidates for surgery, and some operable patients with ES-NSCLC may be better suited for SBRT treatment. Because we currently lack a clear understanding of the biologic features specific to this population, it is crucial to use biology to identify populations of ES-NSCLC that may benefit more from a particular treatment modality. Thus, the goal of this study was to elucidate biomarkers in NSCLC cohorts treated with radiation therapy and surgery to identify resistance to radiation therapy but sensitivity to surgery (or vice-versa) in efforts to delineate whether biomarker-guided clinical decision-making could be used to optimally select patients with ES-NSCLC for SBRT or surgery.

The tumor immune microenvironment (TIME) is becoming increasingly recognized as playing a critical role in the effectiveness of SBRT.[8-10] However, TIME is complex, which is characterized by a diverse range of cell types and intricate spatial distribution. Identifying the key subgroups that influence the efficacy of SBRT necessitates using precise sequencing techniques. Thus, in this work, we attempted to discover new biomarkers for resistance to SBRT using a spatially informed high-plex discovery tool known as digital spatial profiling (DSP). The NanoString GeoMX DSP system enables simultaneous antibody-based detection of multiple proteins from single formalin-fixed paraffin-embedded (FFPE) tissue sections in a quantitative and spatially resolved manner.[11,12] Next, the candidate predictor is further verified by multiplex immunofluorescence (mIF). Unlike from traditional single-color immunohistochemistry (IHC), mIF enables simultaneous detection of diverse protein markers in one tissue slice for the identification of multiple cell phenotypes.[13,14] In this manner, DSP technology can be used as a discovery tool to find spatially resolved protein markers of infiltrating immune cells, stromal cells, and tumor cells associated with resistance to SBRT in ES-NSCLC.

Methods and Materials

Patients and cohorts

This study incorporated 3 cohorts, including a discovery cohort (SBRT cohort) and 2 validation cohorts (SBRT cohort and surgery cohort). The discovery cohort comprised 44 patients with ES-NSCLC (T1-2N0) who received first-line SBRT between 2015 and 2020 and had complete pre-SBRT tumor biopsy specimens. The first external validation cohort consisted of 52 patients with ES-NSCLC treated with SBRT between 2019 and 2022. The predictive performance of the candidate biomarker(s) was further validated in a second validation cohort of 62 patients with T1-2N0 ES-NSCLC who underwent curative-intent lobectomy with mediastinal lymph node dissection. The clinicopathologic data and hematological parameters of all patients were gathered. We systematically recorded complete blood counts, encompassing pretreatment absolute lymphocyte counts (pre-ALC) and posttreatment ALC (post-ALC), absolute neutrophil counts, absolute monocyte counts, and platelet counts. In the SBRT cohort, measurements were obtained within the timeframe starting from the most recent initial day of SBRT (0-2 days from the SBRT initiation) to the latest last day of SBRT (range, −3 to 2 days). In the surgical cohort, measurements were acquired on average within the 3 days preceding the scheduled surgery. Postoperative values were systematically collected within an average of 3 days after the surgery. All patients were followed with a CT or positron emission tomography-CT (PET-CT) 2 to 3 months after radiation therapy, or after the 1-month postoperative assessment for lobectomy. Patients were subsequently followed every 3 to 6 months for the first 2 years and then every 6 months thereafter with CT.

Spatial proteomic analysis

DSP is a novel platform that allows spatially resolved, high-plex quantitative measurement of target proteins on a single FFPE slide. By using DSP, we were able to analyze the expression patterns and spatial distribution of proteins in pre-SBRT tissue samples, providing valuable insights into the prognostic significance of the markers in the context of SBRT treatment. Two continuous tissue slides from the 44 SBRT patients, totaling 88 FFPE whole tissue sections from SBRT cohorts were selected for the DSP experiment. Briefly, the slides were first deparaffinized and subjected to antigen retrieval procedures, then we coincubated them

overnight with fluorescent-labeled antibodies (morphology markers), together with unique photocleavable oligonucleotide-conjugated antibodies (profiling antibodies). In SBRT cohort, 2 serial whole tissue sections were stained with fluorescent-labeled morphology markers (such as epithelial marker pan-cytokeratin [panCK], lymphocyte marker CD3, leukocyte marker CD45, macrophages marker CD68, cancer-associated fibroblasts [CAF] marker α-smooth muscle actin [α-SMA] and nuclear staining SYTO 13). One section was stained with CD3, CD45, panCK, and SYTO 13 to analyze tumor cells, all immune cells, and lymphocytes. The other section was stained with α-SMA, CD68, panCK, and SYTO 13 to profile macrophages cells and stromal cells. For each patient, an average of 12 regions of interest (ROI) were selected according to fluorescence-guided staining characteristics.

The DSP panel included 70 proteins and 6 internal reference (3 housekeepers and 3 background) in Immune Cell Profiling Core, Pan-Tumor Module, Immune Cell Typing Module, IO Drug Target Module, Immune Activation Status Module, Cell Death Module, and PI3K-AKT Module (Table E1). Once the staining step was completed, these slides were loaded in the GeoMx DSP instruments (NanoString) and scanned to produce digital immunofluorescent images of the tissue. For more accurate ROI selection, each tissue was reviewed by the pathologist using hematoxylin and eosin (HE) stained preparations to select representative tumor areas. The pathologist then delineated circular ROIs and custom-drawn ROIs on the entire-tissue IF images. Thereafter, to obtain compartment-specific areas of interest (AOI) protein measurements, we segmented each ROI into 1 or 2 molecularly defined tissue compartments by fluorescent marker colocalization. In the SBRT cohort, 5 molecular compartments were generated: tumor compartment (panCK+), leukocytes compartment (CD45+), lymphocytes compartment (CD3+), macrophages compartment (CD68+), and stroma compartment (α-SMA+). Subsequently, oligonucleotides from the spatially resolved compartments were decoupled on ultraviolet light exposure; collected via microcapillary tube aspiration and deposited into a 96-well plate; hybridized to 4-color, 6-spot optical barcodes; and, finally, digitally quantitated on the nCounter platform (NanoString Technologies).

mIF staining

Any potential biomarker(s) from DSP analysis was further verified by the mIF assay. We developed a mIF protocol (CD44/CD3/panCK/DAPI) using slides from both the discovery cohort and 2 independent validation cohorts to quantify the expression of CD44 and its localization within the tissue samples. FFPE tissues were sectioned at thickness of 4 μm and deparaffinization of tissue sections was done through xylenes and rehydration through decreasing graded alcohol. AR6 buffer was used for antigen retrieval in a microwave oven. Endogenous peroxidase was inactivated by incubation in 3% H_2O_2 for 10 minutes. Multiplex immunohistochemistry was performed by several rounds of staining, each including a protein block with 1% BSA followed by primary antibody and corresponding secondary horseradish peroxidase-conjugated antibody against mouse or rabbit immunoglobulins. The slides were then incubated in different Opal fluorophore (1:100) diluted in 1X Plus Amplification Diluent. After tyramide signal amplification and covalent linkage of the individual Opal fluorophores to the relevant epitope(s), the primary and secondary antibodies were removed via antigen retrieval as previously mentioned and the next cycle of immunostaining was initiated. All slides were counterstained with spectral DAPI and mounted with Antifade fluorescence mounting medium (ab104135, Abcam). We used the Vectra Polaris Imaging System (Akoya Bioscience) to acquire the multispectral imaging and QuPath software to quantify the fluorescence signal as previously described.[15] First, automated tissue segmentation identified panCK+ tumor cells and CD3+ T lymphocytes. CD44 was measured from the CD3+ T lymphocyte compartment, created by binarizing the CD3 signal. The mean fluorescence intensity (MFI) of CD44 was calculated by dividing the target pixel intensity by the area of the CD3+ T lymphocyte compartment.

Data processing

To adjust system-related and experimental bias and to counteract ROI size variation effects, raw digital counts from barcodes corresponding to protein probes were first normalized to internal spike-in controls (external RNA controls consortium, ERCCs). The ROI inclusion criteria were limited to a minimum surface area of 1.6×10^3 μm^2 and minimum nuclei counts of 20 for protein. The quality control (QC) step generated normalization positive factors from individual ROIs. Any ROIs resulting in a normalization positive factor higher than 3 or lower than 0.3 were excluded from the downstream analysis. Finally, downstream analysis was performed on the CD3 compartment of 32 patients, CD45 compartment of 41 patients, CD68 compartment of 40 patients, α-SMA compartment of 37 patients, and tumor compartment of 40 patients, using QC standards. QC-qualified ROI count files were then normalized by the geometric mean of 3 negative isotype controls (mouse immunoglobulin G [IgG] 1, mouse IgG2a, and rabbit IgG). The normalized data were log-transformed with or without being median-centered before comparison and plotting. For further statistical analysis, we averaged the normalized digital counts derived from ROIs of each compartment per patient.

Statistical analysis

All statistical tests were 2-sided, and $P < .05$ was considered statistically significant. Due to the limited number of probes and patients, P values were presented without adjustment. Differences in patient characteristics per group were

calculated by using the Fisher exact test. The Kruskal-Wallis test was used to compare the distribution of panCK, CD45, CD3, CD68, and α-SMA in the 5 molecular compartments. For the differential expression analysis, the nonparametric Mann-Whitney *U* test was implemented.

Follow-up time was calculated from diagnosis to death or the last follow-up using the inverse Kaplan-Meier method. OS was calculated from the date of diagnosis to the date of death from any cause or censored at last follow-up if alive. Recurrence-free survival (RFS) was calculated from the last date of treatment to the date of first recurrence or death or censored at last follow-up if alive without recurrence. Recurrences were defined as new or progressing disease confirmed by imaging or biopsy. Survival curves were calculated according to the Kaplan-Meier analysis and compared by using the log-rank test. OS and RFS between 2 groups were compared using both a univariate and a multivariate Cox regression model, after adjusting for age, Karnofsky performance status (KPS), tumor stage, tumor site, and histology as covariates.[16-21] Univariate and multivariate binary logistic regression models were used to identify the predictors of treatment recurrence. Nearest-neighbor propensity score matching (PSM) (caliper = 0.01) with a 1:1 ratio was conducted based on age, KPS, tumor stage, tumor site, and histology. All data were processed and analyzed in DSP analysis software and R version 4.2.1 with relevant packages. Univariate and multivariate survival analyses were performed using the R packages survival and survminer.

Results

Patient populations

The baseline characteristics of patients with ES-NSCLC in 2 SBRT-treated cohorts are summarized in Table E2. In the SBRT discovery cohort, 25 patients experienced no recurrence and 19 patients developed recurrent disease, of which 9 (47.4%) patients experienced a distant recurrence alone. Notably, lung recurrence was the predominant subtype, accounting for 55.5%, followed by brain recurrence (22.2%), bone recurrence (22.2%), liver recurrence (11.1%), and simultaneous brain and bone recurrence (11.1%). Additionally, 26.3% (5/19) of cases demonstrated local recurrence alone, with an equivalent proportion of cases solely presenting as regional recurrence. In the SBRT validation cohort, 35 cases showed no recurrence and 17 cases experienced recurrence, of which lung recurrence was also the most common. Clinicopathologic features, including age, sex, smoking history, drinking history, KPS, tumor site, histology, tumor stage, and SBRT prescription, did not differ significantly between recurrent and nonrecurrent patients (all $P > .05$). However, recurrent patients consistently showed lower ALC levels, both at baseline and post-SBRT. These differences achieved statistical significance in the SBRT validation cohort, with *P* values of .036 and .046, respectively. Nonrecurrent patients demonstrated a more noticeable ALC percentage change, and recurrent patients experienced a milder reduction in lymphocyte count. Comprehensive information is provided in Table E3. Baseline characteristics of the patients in the surgery cohort before PSM are listed in Table E4. The SBRT and the surgery cohorts exhibited significant differences in TNM stage ($P = .049$) and tumor stage ($P = .032$). Additionally, the surgery group showed a higher percentage of KPS ≥90 and younger age ($P < .001$ for both). Median follow-up was 36.4 months in the SBRT discovery cohort, 31.7 months in the SBRT validation cohort, and 34.2 months in the surgery cohort.

Discovery cohort

We initially evaluated the SBRT cohort using the DSP. Each ROI was compartmentalized in 1 or 2 tissue compartments, from which 70 protein markers (excluding controls) were separately measured, resulting in 70 or 140 candidate biomarkers per ROI. The study design is outlined in Figure 1A. Representative images of the molecular compartments are shown in Figure 1B. The distribution of panCK, CD45, CD3, CD68, and α-SMA in the 5 molecular compartments to confirm the DSP platform effectively profiled tumor, immune and stromal cells, or regions (Fig. 1C).

We then tested 3 different cut-off points (median, tertiles and quantile) to determine their significance. Using the median cut-off point, patients with lower lymphocyte CD44 expression experienced significantly longer RFS (log-rank $P < .001$; Fig. 2A) and OS (log-rank $P = .001$; Fig. E1A). Lymphocyte CD44 could also distinguish recurrent from nonrecurrent patients ($P < .01$ and $P < .05$, respectively; Fig. 2B, C). CD44 expression in tumor cells showed no association with recurrence ($P = .389$; Fig. 1B). On multivariate analysis, lymphocyte CD44 remained statistically significantly associated with unfavorable RFS (hazard ratio [HR], 2.64; 95% CI, 1.41-4.94; $P = .002$; Table 1) and OS (HR, 1.83; 95% CI, 1.05-3.2; $P = .034$; Table E5) after adjusting for age, KPS, tumor stage, tumor site, and histology. Meanwhile, lymphocyte CD44 was predictive of recurrence after SBRT in a multivariate logistic regression model (odds ratio [OR], 3.18; 95% CI, 1.38-7.33; $P = .007$; Table E6). Lymphocyte CD44 was the only biomarker capable of predicting poor survival and recurrence after SBRT. Thus, lymphocyte CD44 was selected for further study and validation.

As the initial step for validation, we aimed to reproduce the DSP findings using fluorescent-based method. Therefore, we evaluated CD44 expression and outcome performance using mIF in the SBRT cohort. Antibodies and fluorophores used in the mIF procedures were detailed in Table E7. Representative images of cell phenotypes acquired with the Vectra system are shown in Figure 2D to 2F. Consistent with DSP findings, lymphocyte CD44 predicted significantly shorter RFS (log-rank $P < .001$; Fig. 2G) and shorter OS (log-rank $P = .004$; Fig. E1C). Recurrent patients

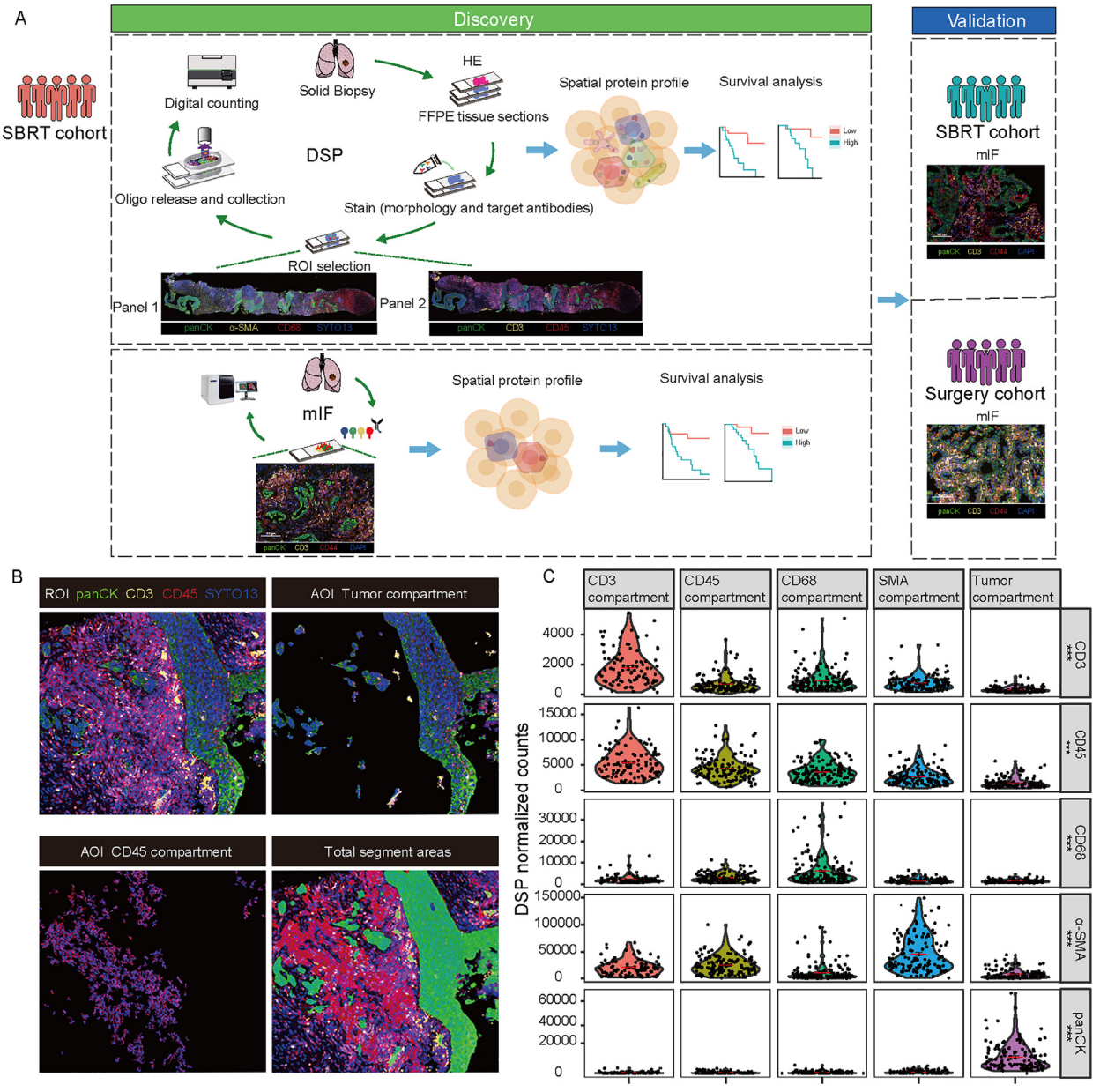

Fig. 1. Overview of methods used to investigate spatial proteome analysis of early-stage non-small cell lung cancer. (A) Schematic representation of the study strategy including the DSP workflow and mIF validation. ROIs were selected based on morphology. Further AOI selection was done within these defined ROIs to investigate different cell types, based on cell surface markers. Representative immunofluorescence and compartmentalized image of consecutive formalin-fixed paraffin-embedded sections (4 μm thickness) from the same tumor formalin-fixed paraffin-embedded block, showing selected ROIs and AOIs. Panel 1: blue, YTO13 (nuclear stain); green, panCK; red, CD68; yellow, α-SMA. Panel 2: blue, YTO13; green, panCK; red, CD45; yellow, CD3. (B) Representative ROI and AOIs (tumor cells and CD45+T cells) collected from the ROI. Colored segments show areas collected for digital counting. (C) DSP normalized counts of panCK, CD45, CD3, α-SMA, and CD68 in the 5 molecular compartments (tumor, CD45, CD3, SMA, and CD68). ***$P < .001$, Kruskal-Wallis test. *Abbreviations:* α-SMA = α- smooth muscle actin; AOI = area of interest; DSP = digital spatial profiling; mIF = multiplex immunofluorescence; panCK = pan cytokeratin; ROI = region of interest.

exhibited a significantly higher percentage of lymphocyte CD44 expression compared with nonrecurrent patients after SBRT ($P < .01$ and $P < .05$, respectively; Fig. 2H, I). The MFI data also revealed high expression tumor cell CD44 of recurrent patients, which was inconsistent with the results from DSP data ($P < .01$; Fig. E1D). Multivariable analysis showed that lymphocyte CD44 remained an independent predictor of RFS and OS (HR, 4.49; $P = .007$ and HR, 7.65; $P = .014$, respectively; Fig. E1E, F). Moreover, high levels of lymphocyte CD44 were significantly associated with recurrence on multivariate logistic regression model (OR, 4.73; $P = .038$; Fig. E1G).

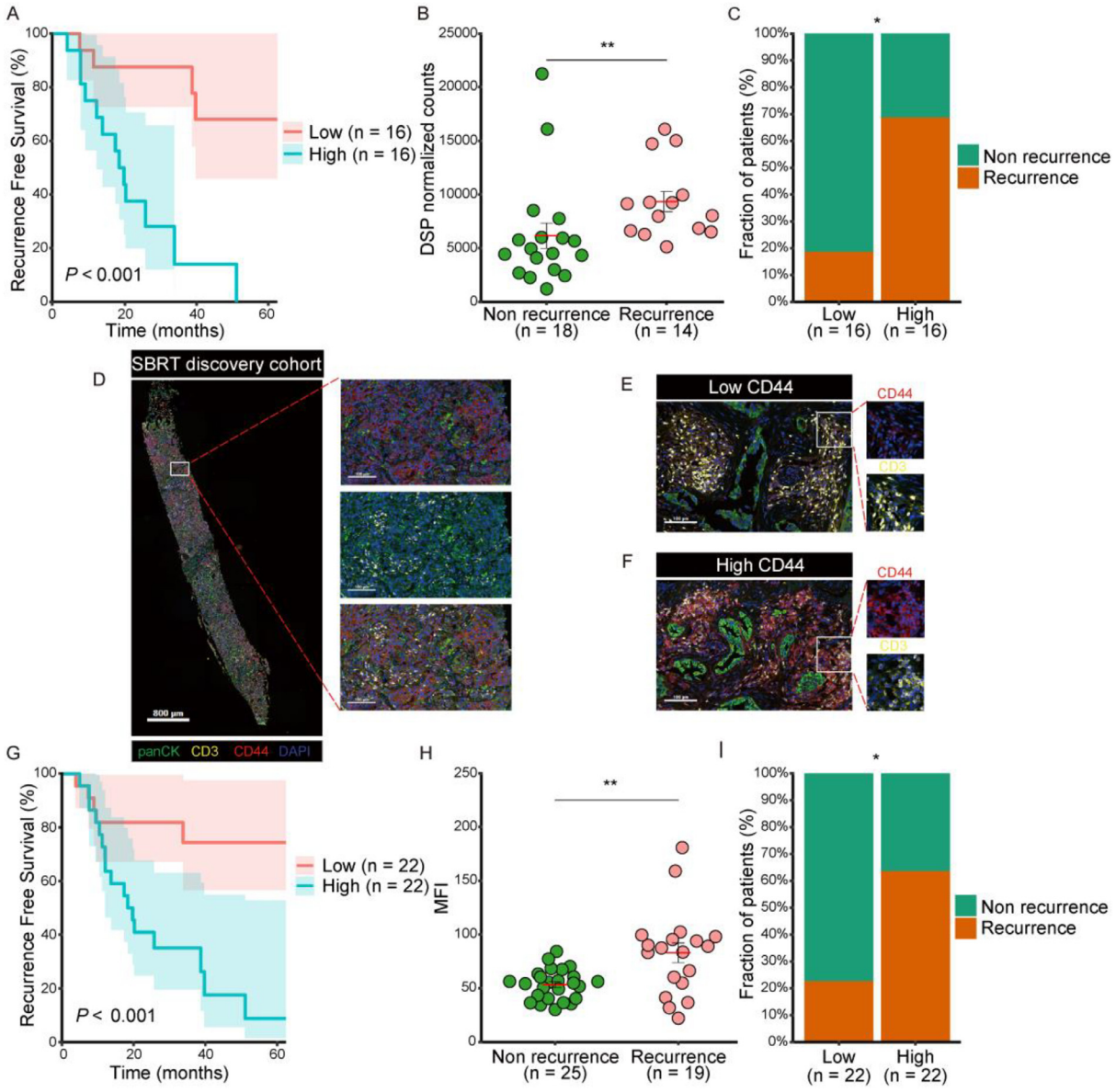

Fig. 2. Identification and validation of lymphocyte CD44 as a potential predictor of poor clinical outcome in SBRT discovery cohort. Kaplan-Meier curve of RFS according to lymphocyte CD44 expression using DSP (A) and MFI (G). Evaluation recurrence to SBRT by lymphocyte CD44 levels using DSP (B) and MFI (H), showing mean ± SEM, $^{*}P < .05$, $^{**}P < .01$, Mann-Whitney *U* test. Proportion of patients who experienced recurrence or nonrecurrence according to their level of lymphocyte CD44 expression classified as high and low using DSP (C) and MFI (I). $^{*}P < .05$, *P* value was calculated using χ^2 test. (D) Representative fluorescence image of a whole tissue section. panCK (green), CD44 (red), CD3 (yellow), DAPI (blue). Representative fluorescence region of low (E) and high (F) CD44 expression in CD3+ T lymphocytes. The scale bar denotes 800 or 100 μm for whole tissue section or representative fluorescence region, respectively. *Abbreviations:* DSP = digital spatial profiling; MFI = mean fluorescence intensity; OS = overall survival; panCK = pan cytokeratin; RFS = recurrence-free survival; SBRT = stereotactic body radiation therapy.

Additionally, both DSP and MFI data indicated significantly elevated levels of lymphocyte CD44 in patients with a history of alcohol consumption ($P < .01$ and $P < .05$, respectively) and those with a high platelet-to-lymphocyte ratio ($P < .01$ and $P < .001$, respectively). Patients with lower pre-ALC levels showed higher levels of lymphocyte CD44. The MFI data were statistically significant ($P < .01$), and the DSP data exhibited a trend but lack significance ($P = .062$). Patients with elevated neutrophil-to-lymphocyte ratio ($P < .01$) and increased systemic immune-inflammation index ($P < .01$) also exhibited increased lymphocyte CD44 expression as measured by mIF (Fig. E2A-H).

Table 1 Markers significantly associated with RFS in the SBRT discovery cohort

Markers associated with RFS benefit								
Compartment	No.	Marker	Cutpoint	Log-rank *P*	Univariate HR (95% CI)	*P*	Multivariate HR (95% CI)	*P*
CD3 compartment	32	CD127	Median	.036	1.28 (1.05-1.57)	.015	2.01 (1.38-2.94)	<.001
		CD44	Median	<.001	1.33 (1.07-1.64)	.009	2.64 (1.41-4.94)	.002
		BCL6	Median	.04	1.3 (1.05-1.6)	.014	1.42 (1.09-1.84)	.008
		Her2	Median	.003	1.36 (1.05-1.77)	.021	1.53 (1.09-2.15)	.013
		Ki-67	Median	.038	1.29 (1.05-1.6)	.017	1.32 (1-1.73)	.046
		Phospho-GSK3B (S9)	Median	.041	1.29 (1.03-1.61)	.026	1.48 (1.06-2.06)	.02
		FAP-alpha	Top tertile	.007	1.29 (1.05-1.58)	.016	1.37 (1.05-1.78)	.022
		OX40L	Top tertile	.037	1.25 (1.04-1.5)	.019	1.30 (1.03-1.63)	.025
CD45 compartment	41	Her2	Top quantile	.011	3.17 (1.23-8.13)	.046	1.42 (1.02-1.98)	.038
CD68 compartment	40	VISTA	Top quantile	.03	1.20 (1.02-1.41)	.026	1.22 (0.99-1.52)	.067
Tumor compartment	40	Phospho-AKT1 (S473)	Median	.004	1.21 (1.03-1.42)	.018	1.21 (1-1.46)	.053

Abbreviations: HR = hazard ratio; RFS = recurrence-free survival; SBRT = stereotactic body radiation therapy.

Validation cohorts

By using the mIF technique, external validation from the SBRT was conducted. Representative images of whole tissue and lymphocyte CD44 expression in the SBRT validation cohort were shown in Figure 3A to 3C. Using the median cut-point, patients with low lymphocyte CD44 expression showed significantly favorable RFS and OS after SBRT (log-rank $P = .013$ and $P = .022$, respectively; Fig. 3D, E). Moreover, high levels of lymphocyte CD44 were significantly associated with recurrence after SBRT ($P < .05$; Fig. 3F). Using the median cut-off, around 81% of CD44-low lymphocyte patients did not experience recurrence, compared with 53.8% recurrence in CD44-high patients ($P = .076$; Fig. 3G). The high expression of CD44 in tumor cells was not associated with SBRT recurrence ($P = .373$; Fig. E3A). On multivariate analysis, lymphocyte CD44 remained an independent predictor of RFS and OS even after adjusting for age, KPS, TNM stage, histology, and tumor site (HR, 3.73; $P = .026$ and HR, 8.50; $P = .041$, respectively; Fig. E3B, C). On the multivariate logistic regression model, lymphocyte CD44 demonstrated a predictive association with post-SBRT recurrence; however, statistical significance was not achieved (OR, 3.43; $P = .096$; Fig. E3D). Consistent with the results in the SBRT discovery cohort, lymphocyte CD44 expression was associated with SBRT resistance and unfavorable survival. Lymphocyte CD44 expression significantly increased in squamous cell carcinoma patients ($P < .05$) and displayed an upward trend in individuals with a history of alcohol consumption (Fig. E3E, F).

Subsequently, validation of lymphocyte CD44 was performed in the surgical cohort. Representative images of whole tissue and lymphocyte CD44 expression in the surgery cohort all illustrated in Figure 4A to 4C. In contrast to the SBRT-treated cohorts, higher lymphocyte CD44 expression were predictive of favorable RFS and OS in the surgically treated cohort (log-rank $P = .003$ and $P = .016$, respectively; Fig. 4D, E). Although statistically insignificant, there was an association observed between lymphocyte CD44 expression and nonrecurrence ($P > .05$ for all; Fig. 4F, G). Low expression of CD44 in tumor cells was also related to postoperative recurrence, but without statistical significance ($P = .058$; Fig. E4A). After adjusting for clinical prognostic factors on multivariate analysis of RFS and OS, lymphocyte CD44 remained statistically significant (HR, 0.31; $P = .004$ and HR, 0.21; $P = .01$, respectively; Fig. E4B, C). Low levels of lymphocyte CD44 were found to be associated with a higher risk of recurrence after surgery, although this association did not reach statistical significance in the multivariate logistic regression model (OR, 0.3; $P = .103$; Fig. E4D).

Comparative analysis

We observed no significant differences in OS and RFS between SBRT versus surgery (log-rank $P = .171$ and $P = .117$, respectively; Fig. 5A, B). By using the median cut-off point, we found that patients with low lymphocyte CD44 expression who received SBRT had better RFS and OS compared with those who underwent surgery (log-rank $P < .001$ for all; Fig. 5C, D). Conversely, patients with high lymphocyte CD44 expression in the surgery cohort exhibited better RFS compared with those in the SBRT cohort (log-rank $P = .016$; Fig. 5E), but there was no significant difference in OS between the 2 treatment groups (log-rank $P = .139$; Fig. 5F). The representative images illustrating the expression of lymphocyte CD44 in the favorable populations of SBRT and surgery are depicted in Figure 5G and 5H.

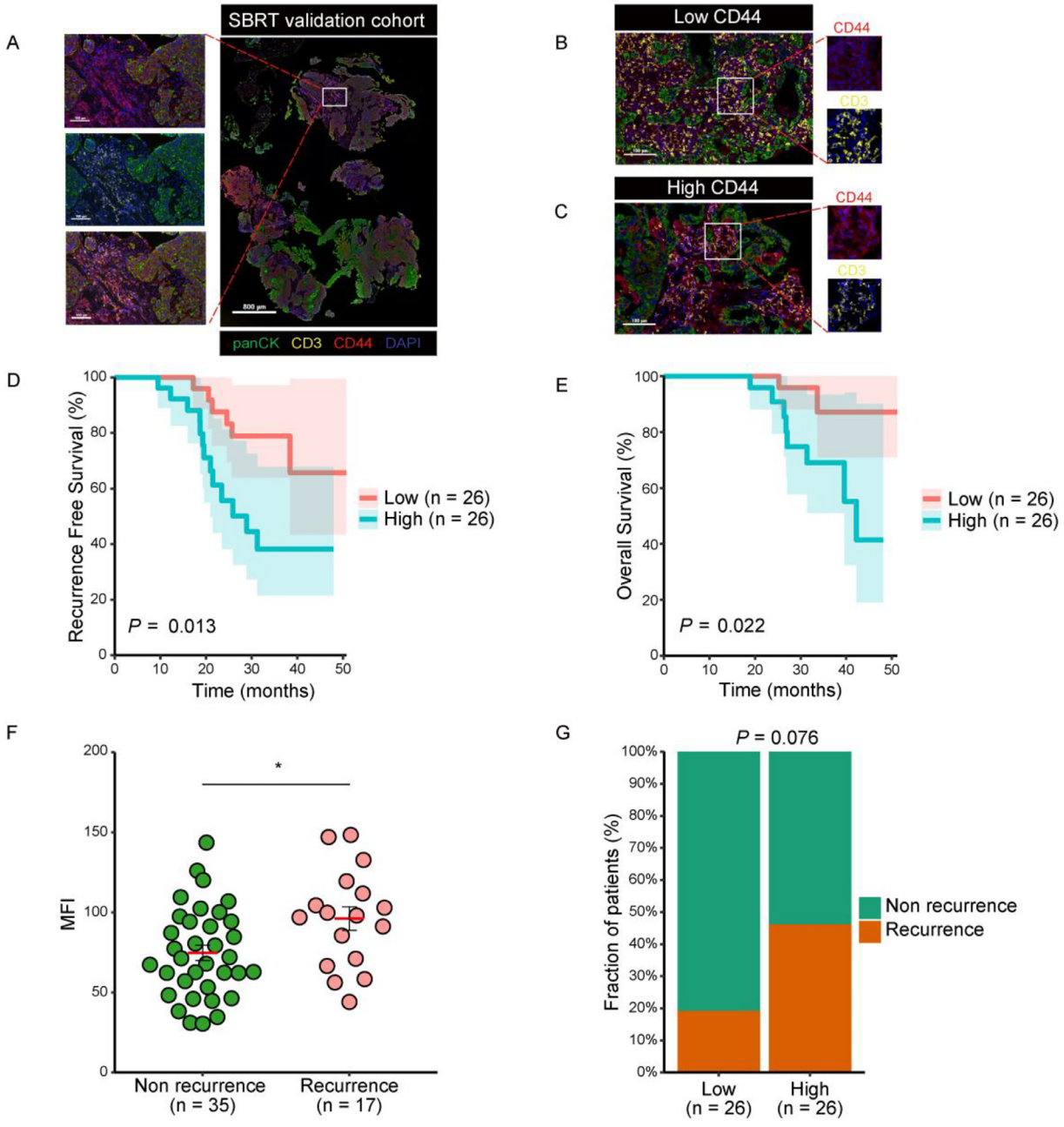

Fig. 3. Validation of lymphocyte CD44 as an indicative biomarker of resistance to SBRT. (A) Representative fluorescence image of a whole tissue section: panCK (green), CD44 (red), CD3 (yellow), and DAPI (blue). Representative fluorescence region of low (B) and high (C) CD44 expression in CD3+ T lymphocytes. The scale bar denotes 800 or 100 μm for whole tissue section or representative fluorescence region, respectively. Kaplan-Meier RFS curve (D) and OS curve (E) according to the lymphocyte CD44 expression measured by MFI. (F) Evaluation recurrence to SBRT by lymphocyte CD44 expression using MFI, showing mean ± SEM, $^*P < .05$, Mann-Whitney *U* test. (G) Proportion of patients who experienced recurrence or nonrecurrence according to their level of lymphocyte CD44 expression classified as high and low. $^*P < .05$; *P* value was calculated using χ^2 test. *Abbreviations:* MFI = mean fluorescence intensity; OS = overall survival; panCK = pan cytokeratin; RFS = recurrence-free survival; SBRT = stereotactic body radiation therapy.

To address the inherent differences in baseline characteristics between the SBRT and surgery groups (such as age, KPS, tumor stage, histology, and tumor site), a PSM model was established (Table E8). After the application of the PSM model, a 1:1 matching was achieved, resulting in 23 patients in both the SBRT and surgery groups. Notably, no significant differences were observed in terms of RFS and OS between the 2 matched groups (Fig. E5A, B). Patients with low expression of lymphocyte CD44 (n = 17) shows significantly longer RFS and OS after SBRT treatment (log-rank

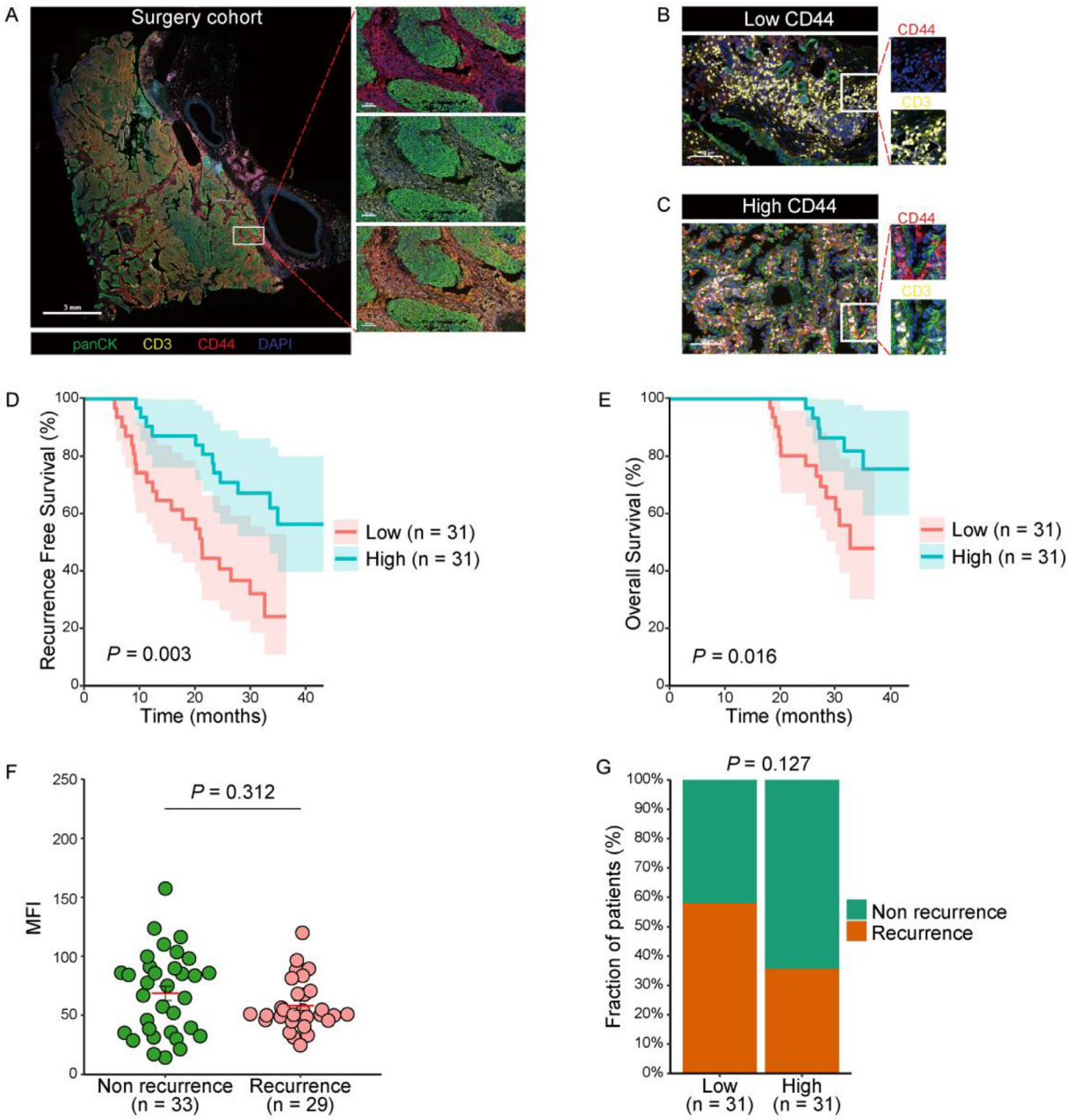

Fig. 4. Identification of lymphocyte CD44 as an indicative biomarker of sensitivity to surgery. (A) Representative fluorescence image of a whole tissue section: panCK (green), CD44 (red), CD3 (yellow), and DAPI (blue). Representative fluorescence region of low (B) and high (C) CD44 expression in CD3+ T lymphocytes. The scale bar denotes 800 or 100 μm for whole tissue section or representative fluorescence region, respectively. Kaplan-Meier RFS curve (D) and OS curve (E) according to lymphocyte CD44 expression using MFI. (F) Evaluation recurrence to surgery by lymphocyte CD44 levels using MFI, showing mean ± SEM, Mann-Whitney *U* test. (G) Proportion of patients who experienced recurrence or nonrecurrence according to their level of lymphocyte CD44 expression classified as high and low. *P* value was calculated using χ^2 test. *Abbreviations*: MFI = mean fluorescence intensity; OS = overall survival; panCK = pan cytokeratin; RFS = recurrence-free survival.

$P < .001$ and $P = .006$, respectively; Fig. E5C, D). Among the patients with high expression of lymphocyte CD44 (n = 29), no significant difference in survival was observed between the SBRT and surgery groups (log-rank $P = .117$ and $P = .613$, respectively; Fig. E5E, F). However, due to the small number of cases after PSM, the differences were not statistically significant.

Lastly, we used PSM to adjust for the differences in covariates between the high and low lymphocyte CD44 expression groups, including variables such as age, KPS, tumor

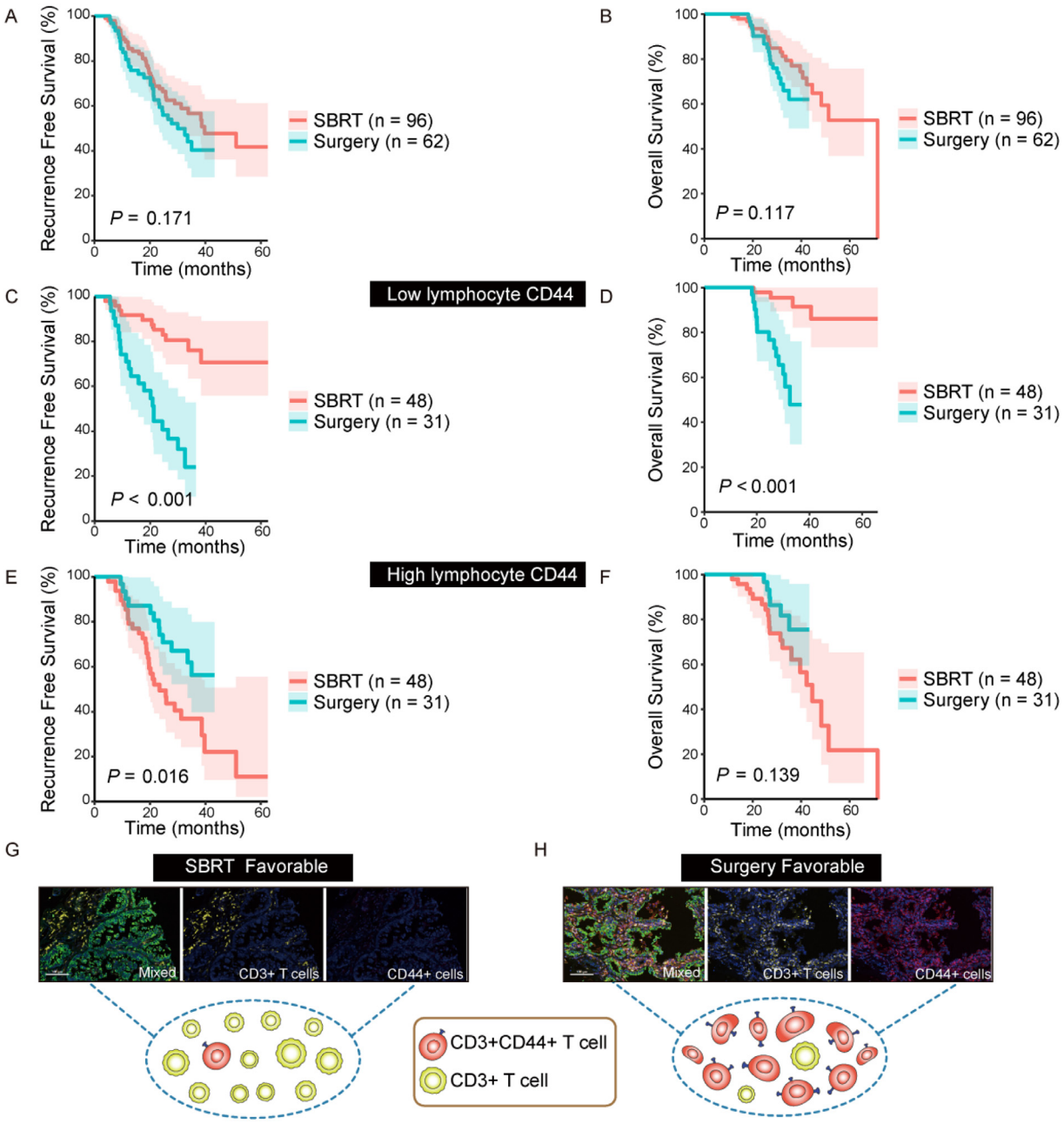

Fig. 5. Lymphocyte CD44 as a differentiator of clinical outcomes in SBRT versus surgery. Kaplan-Meier RFS curve (A) and OS curve (B) between SBRT and surgery groups before PSM. In patients with low lymphocyte CD44 expression, RFS curve (C) and OS curve (D) between SBRT and surgery groups. In patients with high lymphocyte CD44 expression, RFS curve (E) and OS curve (F) between SBRT and surgery groups. Correlation between clinical outcomes and spatial distribution of lymphocyte CD44 in SBRT and surgery cohort. (G) Patients with low expression of lymphocyte CD44 are the favorable candidates for SBRT. (H) Patients with high expression of lymphocyte CD44 are the favorable candidates for surgery. *Abbreviations*: OS = overall survival; PSM = propensity score matching; RFS = recurrence-free survival; SBRT = stereotactic body radiation therapy.

stage, histology, and tumor site (Table E9). After applying PSM, a total of 51 patients were compared. There was no significant difference observed in terms of RFS and OS between the high and low lymphocyte CD44 expression groups (Fig. E6A, B). Among the 64 patients who underwent SBRT, those with low lymphocyte CD44 expression experienced significantly improved outcomes (log-rank $P = .002$ and $P = .004$, respectively; Fig. E6C, D). Among the 38 patients who underwent surgery, patients with high expression of lymphocyte CD44 expression had enhanced outcomes (log-rank $P < .001$ and $P = .003$, respectively; Fig. E6E, F).

Characteristics of tumor-infiltrating CD44-high lymphocytes

To delve deeper into the characteristics of tumor-infiltrating CD44-high lymphocytes, we conducted multicolor immunofluorescence staining on 2 consecutive whole sections from 40 patients with high lymphocyte CD44 expression in the SBRT cohorts. One section was stained with CD3, CD44, CD62L, panCK, and DAPI to analyze tumor cells, effector memory T lymphocytes (CD3+CD44+CD62L−), and central memory T lymphocytes (CD3+CD44+CD62L+). Another section was stained with CD3, CD44, PD-1, Ki-67, panCK, and DAPI to analyze the proliferation and PD-1 expression of CD44-high lymphocytes. Representative fluorescence images are shown in Figure E7A and E7C. Statistical analysis revealed a significantly higher proportion of CD3+CD44+CD62L− cells compared with CD3+CD44+CD62L+ ($P < .001$; Fig. E7B), indicating that most CD44-high lymphocytes exhibit an effector memory cell phenotype. Furthermore, a significant portion of lymphocytes with high CD44 expression did not show Ki-67 and PD-1 expression ($P < .001$; Fig. E7D, E).

Discussion

In the present study, we have demonstrated the potential of DSP technology in identifying spatially informed biologic predictors of resistance to SBRT in ES-NSCLC. Our findings revealed that overexpression of lymphocyte CD44 was associated with unfavorable clinical outcomes, including radiation recurrence, shorter RFS and poor OS in the SBRT cohort. The association between lymphocyte CD44 and these outcomes was further validated using mIF as well as multiple validation cohorts. Of note, this is the first study to address the predictive performance capacity of lymphocyte CD44 in patients with ES-NSCLC treated with SBRT.

CD44 is a cell surface transmembrane glycoprotein that is widely expressed and contributes to cell-cell and cell-matrix adhesion and communication. It is involved in various cellular processes such as cell growth, differentiation, trafficking, and has been found to be highly expressed on cancer stem cells (CSC).[22-25] CD44 interacts with various ECM components such as hyaluronan (HA), osteopontin (OPN), and matrix metalloproteinases (MMPs), promoting tumor growth and metastasis.[26] Recent studies have revealed that the overexpression of CD44 is associated with radiation resistance, lymph node metastasis, recurrence, advanced stage, and poor survival in lung, breast, esophageal, pancreatic, gastric, colorectal, and head and neck carcinoma.[27-36] The CD44 gene regularly undergoes alternative splicing, resulting in the standard (CD44s) and variant (CD44v) isoforms. Extensive studies revealed that both CD44s and CD44v (specifically CD44v6) play different vital roles in enhancing several carcinogenic processes. However, the present study primarily focused on assessing the predictive effect of spatially informed CD44 expression on SBRT. Further investigations are warranted to explore which specific subtypes exert a greater influence on radiation therapy and elucidate the underlying mechanisms through which these subtypes promote resistance to radiation therapy. Because CD44 is a surface glycoprotein, it is potentially amenable for therapeutic antibody-based blockade. For medically unfit EC-NSCLC patients with heightened CD44 expression in lymphocytes, a targeted approach combining CD44 and SBRT could be considered. Conversely, surgically eligible EC-NSCLC patients with elevated CD44 expression in lymphocytes may benefit more from surgical intervention.

Herein, from the analysis of the surgery cohorts, we observed a trend toward improved survival in patients with high lymphocyte CD44 expression, which is consistent with data of operable esophageal cancer.[37,38] This insinuates that biologic factors can be used to optimally select patients for surgery or radiation therapy. Using clinical (nonbiologic) factors, several retrospective studies have provided evidence that certain subgroups of patients may benefit more from one modality than other. For medically operable elderly patients, SBRT could be a better choice than surgery on account of reduced postoperative morbidity and mortality.[39-41] Patients with EGFR mutations have better outcomes after SBRT,[42] but the opposite is true for cases in patients with KRAS mutations.[43] Squamous cell histology,[21] large-sized tumor,[16,18] and centrally located tumors[44-46] may be associated with a higher rate of locoregional failure and metastatic progression after SBRT, for whom surgery could be preferred if feasible.

Despite the abundance of clinical biomarkers, previous studies have been largely deficient in terms of genomic, transcriptomic, and other molecular data in identifying the appropriate patient population for SBRT versus surgery. One of the reasons is that the Cancer Genome Atlas database and large-scale studies have predominantly focused on the molecular feature profiling of surgically resected tumor tissues in NS-NSCLC but lack data in context of SBRT. Based on the analysis conducted using spatial multiomics tools (DSP and mIF), which are strikingly consistent with data from other tumor types,[47,48] we posit that patients with high expression of lymphocyte CD44 could be better served with surgery and patients with low expression with SBRT. Although our results have significant implications for both patients and clinicians, they require validation in larger prospective cohorts.

This study illustrates the potential to leverage high-plex profiling on DSP to identify novel biomarkers associated with clinical response to SBRT. However, there were some limitations in our study. First, this single-center-based study encompassed relatively low sample sizes. The absence of external validation using DSP technology might attenuate the power of our model. Second, retrospective studies have inherent limitations, including the possibility of selection bias and the subjectivity of ROI selection, so these results still need to be interpreted with caution. Third, due to the novelty of DSP technology, data on radiation therapy

cannot be obtained from the public database for extended verification. Lastly, this study does not provide conclusive evidence regarding the mechanism through which lymphocyte CD44 overexpression confers resistance to radiation therapy.

Although lymphocyte CD44 exhibited significant predictive roles in both surgical and SBRT treatment, the specific mechanisms underlying these differences need further exploration. Gaglia et al[49] used the cyclic immunofluorescence (CyCIF) technique to elucidate a network of lymphocyte interactions (lymphonets), highlighting a prominent feature of the anticancer immune response. We plan to next use the CyCIF technique to elucidate whether lymphocyte CD44 forms an interaction network with other cells, aiming to clarify the mechanism of action of lymphocyte CD44.

Conclusion

This study emphasizes the previously unknown association between lymphocyte CD44 expression and resistance to SBRT in ES-NSCLC. Lymphocyte CD44 has the potential to serve as a novel biomarker for the optimal stratification of patients, aiding in the decision-making process between surgery and SBRT for operable ES-NSCLC.

References

1. Henschke CI, Yankelevitz DF, Libby DM, et al. International Early Lung Cancer Action Program Investigators. Survival of patients with stage I lung cancer detected on CT screening. *N Engl J Med* 2006;355:1763-1771.
2. Kovalchik SA, Tammemagi M, Berg CD, et al. Targeting of low-dose CT screening according to the risk of lung-cancer death. *N Engl J Med* 2013;369:245-254.
3. Ettinger DS, Wood DE, Aisner DL, et al. NCCN guidelines insights: Non-small cell lung cancer, version 2.2023. *J Natl Compr Canc Netw* 2023;21:340-350.
4. Nagata Y, Hiraoka M, Shibata T, et al. Prospective trial of stereotactic body radiation therapy for both operable and inoperable T1N0M0 non-small cell lung cancer: Japan Clinical Oncology Group study JCOG0403. *Int J Radiat Oncol Biol Phys* 2015;93:989-996.
5. Timmerman RD, Paulus R, Pass HI, et al. Stereotactic body radiation therapy for operable early-stage lung cancer: Findings from the NRG Oncology RTOG 0618 trial. *JAMA Oncol* 2018;4:1263-1266.
6. Chang JY, Senan S, Paul MA, et al. Stereotactic ablative radiotherapy versus lobectomy for operable stage I non-small-cell lung cancer: A pooled analysis of two randomised trials. *Lancet Oncol* 2015;16:630-637.
7. Chang JY, Mehran RJ, Feng L, et al. Stereotactic ablative radiotherapy for operable stage I non-small-cell lung cancer (revised STARS): Long-term results of a single-arm, prospective trial with prespecified comparison to surgery. *Lancet Oncol* 2021;22:1448-1457.
8. Burnette BC, Liang H, Lee Y, et al. The efficacy of radiotherapy relies upon induction of type I interferon-dependent innate and adaptive immunity. *Cancer Res* 2011;71:2488-2496.
9. Fridman WH, Zitvogel L, Sautes-Fridman C, et al. The immune contexture in cancer prognosis and treatment. *Nat Rev Clin Oncol* 2017;14:717-734.
10. Lee Y, Auh SL, Wang Y, et al. Therapeutic effects of ablative radiation on local tumor require CD8+ T cells: Changing strategies for cancer treatment. *Blood* 2009;114:589-595.
11. Beechem JM. High-plex spatially resolved RNA and protein detection using digital spatial profiling: A technology designed for immuno-oncology biomarker discovery and translational research. *Methods Mol Biol* 2020;2055:563-583.
12. Merritt CR, Ong GT, Church SE, et al. Multiplex digital spatial profiling of proteins and RNA in fixed tissue. *Nat Biotechnol* 2020;38:586-599.
13. Taube JM, Akturk G, Angelo M, et al. The Society for Immunotherapy of Cancer statement on best practices for multiplex immunohistochemistry (IHC) and immunofluorescence (IF) staining and validation. *J Immunother Cancer* 2020;8 e000155.
14. Wilson CM, Ospina OE, Townsend MK, et al. Challenges and opportunities in the statistical analysis of multiplex immunofluorescence data. *Cancers (Basel)* 2021;13:3031.
15. Bankhead P, Loughrey MB, Fernandez JA, et al. QuPath: Open source software for digital pathology image analysis. *Sci Rep* 2017;7:16878.
16. Allibhai Z, Taremi M, Bezjak A, et al. The impact of tumor size on outcomes after stereotactic body radiation therapy for medically inoperable early-stage non-small cell lung cancer. *Int J Radiat Oncol Biol Phys* 2013;87:1064-1070.
17. Bryant AS, Rudemiller K, Cerfolio RJ. The 30- versus 90-day operative mortality after pulmonary resection. *Ann Thorac Surg* 2010;89:1717-1722 discussion 1722-1723.
18. Dunlap NE, Larner JM, Read PW, et al. Size matters: A comparison of T1 and T2 peripheral non-small-cell lung cancers treated with stereotactic body radiation therapy (SBRT). *J Thorac Cardiovasc Surg* 2010;140:583-589.
19. Nonaka M, Kadokura M, Yamamoto S, et al. Tumor dimension and prognosis in surgically treated lung cancer: For intentional limited resection. *Am J Clin Oncol* 2003;26:499-503.
20. van Meerbeeck JP, Kramer GW, Van Schil PE, et al. Randomized controlled trial of resection versus radiotherapy after induction chemotherapy in stage IIIA-N2 non-small-cell lung cancer. *J Natl Cancer Inst* 2007;99:442-450.
21. Woody NM, Stephans KL, Andrews M, et al. A histologic basis for the efficacy of SBRT to the lung. *J Thorac Oncol* 2017;12:510-519.
22. Leon F, Seshacharyulu P, Nimmakayala RK, et al. Reduction in O-glycome induces differentially glycosylated CD44 to promote stemness and metastasis in pancreatic cancer. *Oncogene* 2022;41:57-71.
23. Mani SA, Guo W, Liao MJ, et al. The epithelial-mesenchymal transition generates cells with properties of stem cells. *Cell* 2008;133:704-715.
24. Zhao S, Chen C, Chang K, et al. CD44 expression level and isoform contributes to pancreatic cancer cell plasticity, invasiveness, and response to therapy. *Clin Cancer Res* 2016;22:5592-5604.
25. Zoller M. CD44: Can a cancer-initiating cell profit from an abundantly expressed molecule? *Nat Rev Cancer* 2011;11:254-267.
26. Morath I, Hartmann TN, Orian-Rousseau V. CD44: More than a mere stem cell marker. *Int J Biochem Cell Biol* 2016;81:166-173.
27. Wang SJ, Wreesmann VB, Bourguignon LY. Association of CD44 V3-containing isoforms with tumor cell growth, migration, matrix metalloproteinase expression, and lymph node metastasis in head and neck cancer. *Head Neck* 2007;29:550-558.
28. Auvinen P, Tammi R, Kosma VM, et al. Increased hyaluronan content and stromal cell CD44 associate with HER2 positivity and poor prognosis in human breast cancer. *Int J Cancer* 2013;132:531-539.
29. Smit JK, Faber H, Niemantsverdriet M, et al. Prediction of response to radiotherapy in the treatment of esophageal cancer using stem cell markers. *Radiother Oncol* 2013;107:434-441.
30. Chen Y, Fu Z, Xu S, et al. The prognostic value of CD44 expression in gastric cancer: A meta-analysis. *Biomed Pharmacother* 2014;68:693-697.
31. Jiang H, Zhao W, Shao W. Prognostic value of CD44 and CD44V6 expression in patients with non-small cell lung cancer: Meta-analysis. *Tumour Biol* 2014;35:7383-7389.
32. Li Z, Chen K, Jiang P, et al. CD44V/CD44S expression patterns are associated with the survival of pancreatic carcinoma patients. *Diagn Pathol* 2014;9:79.
33. Ozawa M, Ichikawa Y, Zheng YW, et al. Prognostic significance of CD44 variant 2 upregulation in colorectal cancer. *Br J Cancer* 2014;111:365-374.

34. Yang SZ, Ji WH, Mao WM, et al. Elevated levels of preoperative circulating CD44(+) lymphocytes and neutrophils predict poor survival for non-small cell lung cancer patients. *Clin Chim Acta* 2015;439:172-177.
35. Linge A, Lohaus F, Lock S, et al. HPV status, cancer stem cell marker expression, hypoxia gene signatures and tumour volume identify good prognosis subgroups in patients with HNSCC after primary radiochemotherapy: A multicentre retrospective study of the German Cancer Consortium Radiation Oncology Group (DKTK-ROG). *Radiother Oncol* 2016;121:364-373.
36. Wang CY, Huang CS, Yang YP, et al. The subpopulation of CD44-positive cells promoted tumorigenicity and metastatic ability in lung adenocarcinoma. *J Chin Med Assoc* 2019;82:196-201.
37. Bottger TC, Youssef V, Dutkowski P, et al. Expression of CD44 variant proteins in adenocarcinoma of Barrett's esophagus and its relation to prognosis. *Cancer* 1998;83:1074-1080.
38. Honing J, Pavlov KV, Meijer C, et al. Loss of CD44 and SOX2 expression is correlated with a poor prognosis in esophageal adenocarcinoma patients. *Ann Surg Oncol* 2014;21(suppl 4):S657-S664.
39. Chen H, Louie AV, Boldt RG, et al. Quality of life after stereotactic ablative radiotherapy for early-stage lung cancer: A systematic review. *Clin Lung Cancer* 2016;17:e141-e149.
40. Poghosyan H, Sheldon LK, Leveille SG, et al. Health-related quality of life after surgical treatment in patients with non-small cell lung cancer: A systematic review. *Lung Cancer* 2013;81:11-26.
41. Rosen JE, Salazar MC, Wang Z, et al. Lobectomy versus stereotactic body radiotherapy in healthy patients with stage I lung cancer. *J Thorac Cardiovasc Surg* 2016;152:44-54.e9.
42. Blumenfeld PA, Kreinbrink PJ, Marwaha G. Stereotactic body radiation therapy outcomes for early stage and oligometastatic non−small cell lung cancer based on molecular profile. *Int J Radiat Oncol Biol Phys* 2017;98:230.
43. Mak RH, Hermann G, Lewis JH, et al. Outcomes by tumor histology and *KRAS* mutation status after lung stereotactic body radiation therapy for early-stage non-small-cell lung cancer. *Clin Lung Cancer* 2015;16:24-32.
44. Bezjak A, Paulus R, Gaspar LE, et al. Safety and efficacy of a five-fraction stereotactic body radiotherapy schedule for centrally located non-small-cell lung cancer: NRG Oncology/RTOG 0813 trial. *J Clin Oncol* 2019;37:1316-1325.
45. Kimura T, Nagata Y, Harada H, et al. Phase I study of stereotactic body radiation therapy for centrally located stage IA non-small cell lung cancer (JROSG10-1). *Int J Clin Oncol* 2017;22:849-856.
46. Timmerman R, McGarry R, Yiannoutsos C, et al. Excessive toxicity when treating central tumors in a phase II study of stereotactic body radiation therapy for medically inoperable early-stage lung cancer. *J Clin Oncol* 2006;24:4833-4839.
47. Wu CT, Lin WY, Chang YH, et al. Impact of CD44 expression on radiation response for bladder cancer. *J Cancer* 2017;8:1137-1144.
48. Karamitopoulou E, Wenning AS, Acharjee A, et al. Spatially restricted tumour-associated and host-associated immune drivers correlate with the recurrence sites of pancreatic cancer. *Gut* 2023;72:1523-1533.
49. Gaglia G, Burger ML, Ritch CC, et al. Lymphocyte networks are dynamic cellular communities in the immunoregulatory landscape of lung adenocarcinoma. *Cancer Cell* 2023;41:871-886.e10.